Full Paper

Propellants, Explosives, Pyrotechnics

DOI: 10.1002/prep.202000328

Thermocouple Temperature Measurements in Metalized Explosive Fireballs

David L. Frost,*[a] John-Mark Clemenson,[b] Samuel Goroshin,[a] Fan Zhang,[c] and Michael Soo[b]

Abstract: The detonation of a metalized explosive generates a fireball that has a spatially non-uniform distribution of particle concentration and gas temperature. The transient gas temperature field must be probed with ruggedized spatially- and temporally-resolved diagnostics. The use of in-situ thermocouples for temperature measurements within multiphase fireballs is demonstrated. Although the thermocouple temperature lags behind the local gas temperature, the transient gas temperature is assessed by modeling the sensor assuming first-order response and using two analysis methods: (1) when the thermocouple temperature trace reaches a local extrema, the thermocouple temperature is instantaneously equal to the local gas temperature, and (2) reconstructing the gas temperature trace using multiple co-located thermocouples of different lag responses. The temperature history within the fireball at various distances is presented for charges consisting of packed beds of particles saturated with liquid nitromethane. The results for reactive particles (Al, Ti, Zr) are compared with non-reactive particles (Fe), as well as homogeneous NM charges. For NM charges, a maximum gas temperature of about 1100 K occurs at times on the order of 100's of milliseconds, less than the temperature of the burning soot in the fireball (~1900 K). With Al particles, the gas temperature is spatially non-uniform due to particle jetting and non-uniform particle combustion, but gas temperatures up to about 1800 K are recorded for times up to 0.5 s, less than the temperature of the burning particles (~2700 K). Inert particles act as a heat sink and the thermocouple temperatures recorded did not exceed 400 K.

Keywords: Metalized explosive · Fireballs · Thermocouple temperature measurements

1 Introduction

1.1 Reaction of Metal Particles in Heterogenous Explosives

The detonation of a homogeneous, oxygen-deficient explosive generates products that can be further oxidized by the oxygen in the surrounding air thus increasing the strength of the blast wave and the fireball temperature. For example, the detonation of oxygen-deficient TNT or nitromethane generates large amounts of carbon monoxide and carbon (soot) that can react with the surrounding air in the mixing zone at the outer region of the expanding fireball. The rate of combustion of the detonation products depends primarily on the rate of mixing with the air and hence is strongly influenced by the charge scale and geometry, as well as by reflected shock waves that perturb the mixing zone. The picture becomes considerably more complex for heterogeneous explosives containing added metal particles. Metals such as aluminum are capable of prompt and highly exothermic reactions with oxidizing products of a high explosive detonation such as water vapour and carbon dioxide, which contributes to the strength of the initial blast wave [1]. Products from these reactions include potential fuels such as hydrogen, carbon monoxide, and soot that together with unreacted aluminum can continue to burn with oxygen near the periphery of the fireball, releasing an additional amount of heat. The sum of this heat and the heat released earlier from aluminum reactions with the detonation products is equal to the energy that can be produced by direct combustion of the aluminum in air.

Experimental evidence suggests that for aluminized charges with a mass on the order of 1 kg and larger, with a moderate metal loading (less than 20% by mass), practically all the aluminum, over a wide particle size range, is consumed in reactions with the detonation products during the very early stages of fireball expansion [1]. In contrast, charges with a very large metal loading, such as packed beds of metal powders saturated with liquid nitromethane, have an insufficient quantity of oxidizers within the products to fully oxidize the aluminum, and the large mass of metal serves as a heat sink to further reduce the temperature of the combustion products. The efficiency of the

[a] *D. L. Frost, S. Goroshin*
Dep't. of Mech. Eng., McGill University
Montreal, Quebec, Canada, H3 A 0 C3
**e-mail: david.frost@mcgill.ca*
[b] *J.-M. Clemenson, M. Soo*
Naval Surface Warfare Center Indian Head Division
Indian Head, MD, USA, 20640
[c] *F. Zhang*
Defence Research and Development – Suffield
Medicine Hat, Alberta, Canada, T1A 8K6

metal reaction, in this case, depends primarily on ignition of the particles and subsequent combustion directly in the hot shocked air surrounding the combustion products. In some cases, particle ignition is delayed, resulting in turbulent flame propagation through the dispersed metal dust cloud [2]. Larger metal particles may not rely only on the turbulent mixing with air as they can penetrate the contact surface between the detonation products and air due to inertia. By burning directly in the air outside the gaseous fireball, these metal particles can contribute to the strength of the blast wave at longer distances [3].

1.2 The Challenge of Temperature Measurements in Explosive Fireballs

Investigation of the complex, multistage nature of metal reaction in explosive fireballs requires in-situ measurements of the fireball parameters including measurements close to the charge. Although pressure measurements are ubiquitous for characterizing explosive performance, they are unreliable at short distances from the charge due to large signal fluctuations caused by the asymmetry of the explosion, particle jetting effects, and the spurious signals produced by particle impacts on the gauge stand or directly on the gauge face [4]. Most prior work in measuring temperatures associated with detonation fireballs have attempted to use non-intrusive optical techniques such as pyrometry or spectrometry to infer the temperature of condensed and gaseous species [5–7]. Given the high opacity of fireballs of fuel-rich and metalized explosives, non-intrusive collection of the emitted light by optical sensors placed outside fireballs probe only temperatures in the outer layer of the fireball. Since radiant emission is strongly dependent on temperature, optical emission measurement techniques are always biased towards the highest temperature in a fireball [8]. For a homogeneous, oxygen-deficient explosive such as nitromethane, the highest temperature is associated with the diffusive flamelets at the mixing interfaces of detonation products with air. Hence, emission measurements typically yield the adiabatic temperature of the stoichiometric mixture of combustion products with air, which has no connection with the temperature inside the fireball [6]. With metalized explosives, the temperature measured by outside optical sensors is similarly associated with the high-temperature diffusive micro-flames surrounding burning particles. Thus, it remains constant and does not reflect the temporal history of the temperature inside the fireball [9].

Optical sensors acquiring continuous emission spectra of condensed species inside the fireball face similar challenges as the measurements are biased towards a few hot spots having a considerably higher temperature than the surrounding gas. Emission spectroscopy can be also used to record the molecular emission bands of some gaseous molecular species such as AlO. The temperature of these excited species can then be estimated by fitting the molecular spectra to theoretical predictions at a given temperature. This kind of measurement is characterized by typical errors on the order of several hundred Kelvin [10]. To estimate the average temperature of non-excited gaseous species in the interstitial space between burning particles, it is necessary to use absorption spectroscopy techniques [11,12]. However, the use of absorption spectroscopy in field experiments that requires placing laser emitters and the light collection optics inside the fireball is extremely challenging. The large and constantly changing optical density makes it difficult to choose an appropriate path length between the laser and the light collection system for a good signal-to-noise ratio [13]. In addition, optical probes are relatively expensive and are difficult to protect. Consequently, they are ill-suited for the multipoint, distributed measurements that are necessary in the spatially non-uniform and potentially asymmetrical environment generated by the detonation of heterogeneous explosives.

1.3 Overcoming the Thermal Inertia Associated with Thermocouple Measurements

The use of thermocouples is a well-established technique for measuring gas temperature at a point in a wide range of fluid systems. To interpret data from thermocouple measurements in an environment characterized by a rapidly changing temperature such as within a fireball, it is, however, necessary to account for the thermocouple inertia. It is the size of the thermocouple junction that mainly controls the degree of thermal lag between the thermocouple and the surrounding flow. Fine thermocouples respond more quickly to changes in the local temperature field but are less robust than thicker thermocouples and can be easily broken. Relatively little work has been carried out using thermocouples embedded within the fireball produced by a homogeneous or heterogeneous explosive. Asay et al. [14] reviewed past work on the use of thermocouples within condensed phase energetic materials and highlighted the issues related to thermocouple response time to perturbations of the local temperature field.

The thermocouple thermal inertia can be, however, accounted for and the real temperature of the flow can be recovered by using interpolation of thermocouple signals from several thermocouples with different junction sizes together with theoretically determined corrections that use, in addition to the signal amplitude, its derivatives. One feature of a thermocouple that is not particularly appreciated in the literature is that while the temperature of a thermocouple junction, in general, lags behind the fast-changing gas temperature [15], it reacts practically instantaneously to changes in the local gas temperature. This feature is independent of the thermocouple junction size and can only be degraded by the signal noise when the change of the signal becomes undetectable.

The effectively instantaneous thermocouple response to a sudden temperature change is demonstrated in a simple experiment in which two co-located thermocouple probes are plunged into a liquid sulfur bath having a temperature of about 433 K. One thermocouple consisted of a thin 12.7 μm foil, whereas the other had a junction size of about 0.8 mm. The resulting temperature histories of the two thermocouples are shown in Figure 1. Note that while the larger thermocouple takes a longer time to come into thermodynamic equilibration with the surrounding fluid, both thermocouple signals begin to rise at effectively the same time.

As the primary mechanism of heat transfer between a thermocouple and the surrounding gas is thermal conduction, the response of a thermocouple is often modeled as a first-order lag system [16] that satisfies the ordinary differential equation:

$$T_{gas} = T_{TC} + \tau T'_{TC} \quad (1)$$

where T_{gas} is the temperature of the surrounding gas, T_{TC} is the thermocouple temperature, τ is the time constant of the system, and T'_{TC} is the time derivative of the thermocouple temperature trace. The first-order simulation with Equation (1) of the thermocouple response to a step-like change of the gas temperature is shown in Figure 1 by dotted lines.

It also follows from approximation (1) of the system dynamic response that, when the thermocouple trace experiences a local minimum or maximum (i.e., $T'_{TC} \approx 0$), the instantaneous temperature of the gas is equal to the thermocouple temperature, regardless of the unknown time constant of the thermocouple. Hence, the *Local Extrema Method* (LEM) of analysis permits the use of the numerical derivative of thermocouple traces to determine the gas temperature at a limited number of temporal points. An example of the LEM analysis is shown in Figure 2 demonstrating the theoretically calculated response of thermocouples with junctions of different sizes exposed to a transient gas temperature having a Friedlander waveform. The peaks in the thermocouple traces are shown to correspond to points in time where the thermocouple temperature and gas temperature are equal.

This simple analysis also reveals an important aspect about the thermocouple response, i.e., if the values of T_{TC} and T'_{TC} in (1) can be determined from the thermocouple trace, then the entire gas temperature trace can be numerically reconstructed if the time constant τ is known *a priori*. In turbulent flows, the thermocouple response time constant depends on the largely unknown flow characteristics. In this case, it can be estimated by a technique that uses multiple thermocouples with different junction sizes placed within proximity. The temperature results from the multiple thermocouples can be extrapolated at any given time to a zero-sized junction to estimate the real gas temperature. The simplest linear extrapolation was used by Julien et al. [17] in an attempt to estimate the radiative heating ahead of a flame propagating in a large aluminum dust cloud as well as in [16] to resolve thermal turbulence in a heated airstream. These works show that the *Numerical Reconstruction Method* (NRM) can be yet another powerful tool to examine transient temperature features of the flow, even in the absence of a well-characterized thermocouple time constant.

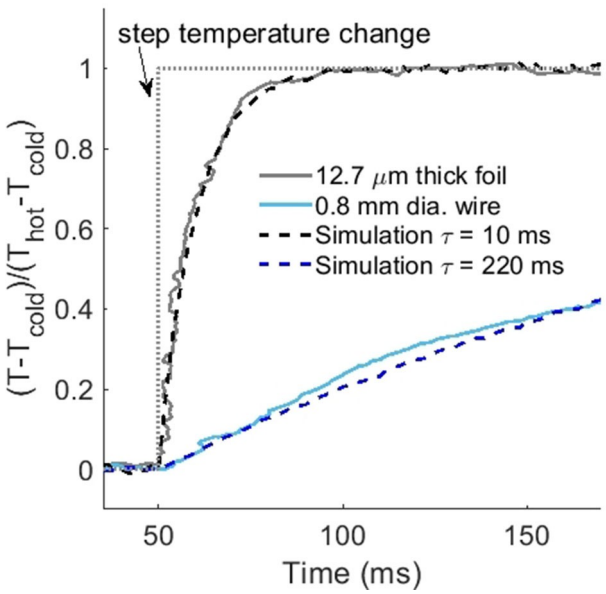

Figure 1. Temperature recorded with two thermocouple probes simultaneously immersed in a bath of molten sulfur, heated to a temperature of 433 K. The fast-response thermocouple consisted of a thin-film based gauge whereas the thermocouple with the slower response had a junction thickness of 0.8 mm.

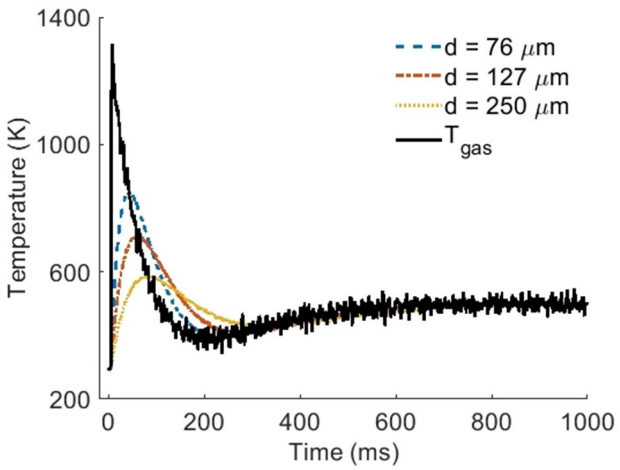

Figure 2. Theoretical response of different sized thermocouples to a Friedlander thermal waveform with reconstruction using multiple thermocouples (the original thermal waveform and reconstruction overlap). Note the extrema of the thermocouple traces are located at points where the thermocouple and gas temperatures are equal.

The present paper presents an analysis of thermocouple temperatures in fireballs of homogeneous and heterogeneous explosives loaded with reactive and non-reactive particles. The homogeneous explosive was comprised of sensitized nitromethane (NM), whereas the heterogeneous charges contained a packed bed of either reactive or inert particles saturated with NM. The results for the gas-phase temperatures within the fireball using the LEM and NRM analyses show a striking contrast with earlier pyrometric measurements of the temperature of the condensed species on the fireball surface using an externally-placed pyrometer [6].

2 Data Analysis Methods

As was mentioned above, several methods that allow extraction of the real gas temperature from transient signal traces recorded with thermocouples of different sizes positioned at the same spatial location have already been discussed in the literature. These methods were analyzed and modified resulting in the original data processing software used in the present paper.

2.1 Local Extrema Method (LEM) Analysis

The simulated thermocouple traces shown in Figure 2 illustrate how the LEM method may be used to determine the instantaneous gas temperature. The derivatives of the noisy traces (T'_{TC}) are first calculated in MATLAB using the Savitzky-Golay method [18] with a user-defined window to remove the effects that noise may have on producing false local extrema. The extrema are then determined by points where T'_{TC} crosses a zero value (any minima or maxima). The resulting crossover points are shown at the intersections of the T_{gas} and T_{TC} traces, showing that the thermocouple temperature equals the instantaneous gas temperature only when the thermocouple temperature exhibits a local minimum or maximum.

2.2 Numerical Reconstruction Method (NRM) Analysis

Another useful technique to analyze thermocouple data is the determination of the gas temperature field by the numerical solution of Equation (1), using the available thermocouple trace, a time constant, and the numerical derivative of the thermocouple data. Determination of the time constant needed to reconstruct accurate gas temperatures is often difficult due to the dependence of the time constant on flow conditions and is not likely to succeed without measuring flow characteristics simultaneously [19]. A technique that can be used to overcome this limitation is blind sensor characterization using at least two co-located thermocouples of different response times. In principle, co-located sensors provide two different dynamic responses of the same gas temperature function. Therefore, the solutions for time constants that satisfy this constraint can be determined by optimization.

The reconstruction of the gas temperature from temperature traces of two sizes of co-located thermocouples is performed in MATLAB using the method outlined by Tagawa et al. [19]. In this preliminary analysis, the following assumptions are made: 1) the thermocouples are co-located such that they experience the same gas temperature and gas velocity, and 2) the thermocouple has a single-valued time constant over the time period of interest. The degree to which these assumptions hold depends largely on the flow conditions and this issue is not addressed in this simple analysis. The intention is to demonstrate the usefulness of this technique to examine the transient thermal characteristics of the flow field.

The thermocouple traces are first smoothed using a Savitzky-Golay filter in combination with outlier removal functions. The sensitivity of filtering and smoothing is user determined to retain prominent features from each thermocouple trace while removing extraneous points and minimizing Gaussian noise. Derivatives are calculated using the Savitzky-Golay method [18]. The reconstruction algorithm performs the calculation of gas temperatures (T_{gi}) for each of the thermocouples given a constrained initial guess value for each of the time constants (τ_i) as shown in Eqs. 2 and 3.

The algorithm returns the time constants that minimize the norm of the difference between the two calculated gas temperatures (Eq. 4), or effectively, when the calculated gas temperatures are equal to the greatest extent possible, over a user-defined time period with a given single-valued time constant constraint.

$$T_{g1} = T_{TC1} + \tau_1 T'_{TC1} \tag{2}$$

$$T_{g2} = T_{TC2} + \tau_2 T'_{TC2} \tag{3}$$

$$e = \sum_{t=0}^{t=t_1} [(T_{g1} - T_{g2})^2] \tag{4}$$

An example of this analysis using the reconstruction of the simulated thermocouple data of a Friedlander form is shown in Figure 2, superimposed with the original function. The noise seeded into the thermocouple simulations is amplified by the reconstruction which requires an increased number of points in the calculation of the derivative to smooth out the noise. The increase in points in the derivative calculation increases the effective smoothing applied to the reconstructed gas temperature which degrades the high frequency features.

3 Experimental Setup

3.1 Explosive Charges and Metal Powders

The charge casings consisted of globe-style light bulbs (12.3 cm dia) cut near the base to remove the filaments. Details of the charge preparation and experimental procedure can be found in [20]. Fireball temperatures were recorded for trials using NM charges (the NM was sensitized with the addition of 10% triethylamine to make it cap sensitive) as well as charges containing a packed bed of solid particles saturated with sensitized NM. A table containing the different inert and reactive particles in the charges is shown in Table 1.

The morphology of the reactive particles is illustrated in the SEM micrographs shown in Figure 3. Except for the glass and aluminum particles, all of the particles have an irregular morphology. The larger titanium and zirconium particles have a fine-scale surface structure with some evidence of micro-porosity. The large (400–600 μm) zirconium particles may be described as sponge-like particles.

3.2 Test Site Configuration

The explosive testing was performed at DRDC Suffield over a multi-year period. The experimental setup is shown in Figure 4. A charge was placed on a 3.5×3.5 cm wooden post at a height of about 1.5 m from the ground. Thermocouple gauges (shown in the right of Figure 4) were placed around the charge at combinations of three different radial standoff distances (combinations of 0.9 m, 1.2 m, and 1.5 m, and 1.9 m) depending on the test.

An example of the mounting of the thermocouples is shown in the photographs in Figure 4. The mounting hardware includes a split-piece thermocouple holder that protects the thermocouple ceramics and the connector from direct fragment and particle impacts while still exposing the bare-wire thermocouple junction to the turbulent flow-

Table 1. Properties of particles used in present experiments; d = particle diameter, m_p = total mass of particles, m_{NM} = mass of nitromethane.

Mat.	d (μm)	m_p (g)	m_{NM} (g)	Morphology	Model
Glass (inert)	100	1506	350	spherical	Ballotini impact beads
Iron (inert)	$44 < d < 149$	2100	750	irregular	Fe-112[a]
Al, a	54	1460	360	spherical	H-50[b]
Al, b	4.5	1460	360	spherical	H-2[b]
Ti, a	$d < 149$	1678	596	irregular	Ti-109[a]
Ti, b	$d < 44$	2044	494	irregular	Ti-104[a]
Zr	400-600	2048	624	irregular	ZR-105[a]

[a] Atlantic Equipment Engineers (NJ). [b] Valimet (CA).

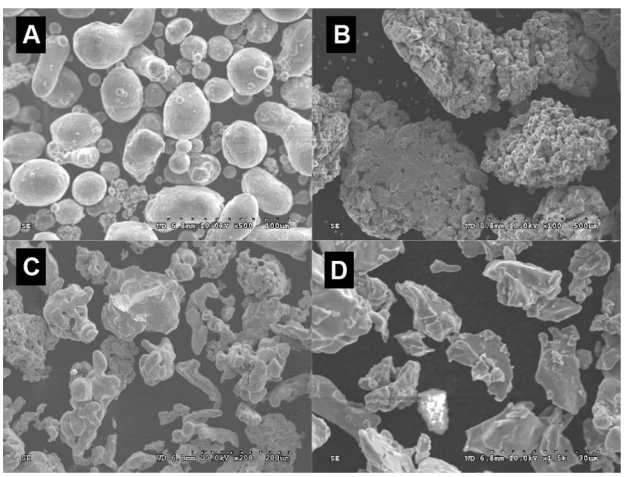

Figure 3. Scanning electron micrographs of the reactive particles used in the present experiments: A) aluminum (H-50), B) zirconium (ZR-105), C) titanium (TI-109), and D) titanium (TI-104).

Figure 4. Top: photograph of the test site with 6 lollipop-mounted pressure gauges and 3 thermocouple stands. Bottom: thermocouple stand and mounting arrangement. The inset images show close-ups of the thermocouple mounts with the single- and multi-thermocouple arrangements.

field. The protection enhances survivability of the thermocouple in the harsh environment of the particle-laden explosive fireballs and allows the reuse of thermocouples for multiple tests.

The majority of the trials utilized 127 μm (0.005″ wire diameter) K-type thermocouples. Smaller 25 μm (0.001″) and 51 μm (0.002″) junction thermocouples were used in a smaller number of experiments. Although finer thermocouples respond more rapidly to the transient ambient temperature, they rarely survived the complete event.

In later tests, a specially designed protective mount, with three thermocouples of different sizes located less than 0.5 cm apart, was implemented in an attempt to implement the NRM analysis of the gas temperature of the flow field. An example implementation of the modified sensor head is shown in the bottom left of Figure 4 with C-type thermocouples. In the tests described in this paper, three K-type thermocouples were used in the sensor head, combined with high bandwidth amplifiers, and had nominal wire diameters of 76, 127, and 250 μm.

4 Results and Discussion

4.1 Reactive and Inert Particle Loadings

Figure 5 presents a selection of high-speed video images illustrating the range of fireball features observed for the various homogeneous and heterogeneous charges used in the present tests. The detonation of a homogeneous charge containing 1 kg of sensitized NM is shown in Figure 5A. The products are highly luminous for the first several hundred microseconds before the products expand and cool. As the detonation products mix with the surrounding air, promoted by the Rayleigh-Taylor instability of the combustion products interface visible after about 1 ms, the soot in the products begins to burn after about 10 ms and continues to burn on a timescale of 100's of milliseconds.

Figure 5B shows single frames from the video record of the explosive dispersal of FE-112 iron particles. No combustion of the iron particles occurs. The luminous region near the top of the particle cloud is due to jetting of the C4 detonation products out of the vertical tube placed into the charge to facilitate the insertion of the detonator into the C4 burster. The air blast wave is visible just outside of the dispersed particle cloud against the horizon near the top of the last frame in the sequence.

For heterogeneous charges containing a packed bed of H-50 (54 μm) spherical aluminum particles, the fraction of the aluminum powder that burned at early times varied from one trial to the next. Figure 5C shows a case where the majority of the aluminum powder reacts uniformly within the fireball, with some unburnt powder visible at the bottom of the fireball. In other trials, there were spatial regions where the particles failed to burn at early times, although they would often burn out by propagation of a flame through the unburnt dust regions at later times.

The large zirconium particles always reacted promptly in all tests (Figure 5D). One feature of the fireball surface for charges with zirconium particles is the formation of stable Rayleigh-Taylor plumes on the combustion products interface visible in Figure 5D. We have speculated earlier that the energy deposited in the fireball by the metal particle combustion reduces the deceleration of the product interface, which slows the growth of the RT instability plumes [21]. Another feature that is evident from Figure 4D is the curved luminous line visible just to the left of the product interface in the 4th frame. This luminous line is associated with the impact of the zirconium particles with the zebra-striped plate behind the charge. Particles that impact the plate fracture into fine fragments which continue to burn and enhancing the luminosity. Figure 4E shows a far-field view of the same trial as in Figure 4D and illustrates that the zirconium particles that are dispersed by the explosion continue to burn as they travel 10's of meters.

Charges containing titanium particles showed different behaviors, depending on the particle size. In the case of the larger TI-109 particles (<149 μm), the particles dispersed uniformly and the onset of reaction of the particles occurred in the earliest video frames, less than 100 μs after detonation of the charge, as shown in Figure 5F. The development of the RT plumes on the fireball interface is essentially the same as observed for the charges with zirconium particles (Figure 5D).

In contrast, Figure 5G shows that the smaller TI-104 titanium particles (<44 μm) do not disperse uniformly, perhaps due to nonuniform force chains between the irregularly-shaped particles, and do not react immediately upon dispersal. Rather, it appears that the particles ignite in local hot spots and a flame propagates through the dispersed powder. As a result, it takes 10's of milliseconds for the majority of the titanium powder to react.

The variations in the particle reaction behavior observed for the various charge conditions exhibited in Figure 5 will influence the uniformity of the temperature field within the fireball, as well as the peak gas temperatures attained. For the light Al particles that have a long residence time within the fireball, high gas temperatures are expected. For larger and heavier Ti and Zr particles, the higher inertia of the particles will allow them to penetrate the combustion products interface quickly and move into the surrounding atmosphere, which limits the time available for energy transfer from the particles to the combustion products. The spatial uniformity of the particle ignition and combustion is expected to influence the spatial uniformity of the fireball gas temperature field. In this respect, we would expect that large Zr and Ti particles would lead to a smaller variation in gas temperature within the fireball, whereas Al and small Ti particles that disperse nonuniformly and burn in a spatially non-uniform manner should generate a larger variation in gas fireball temperatures.

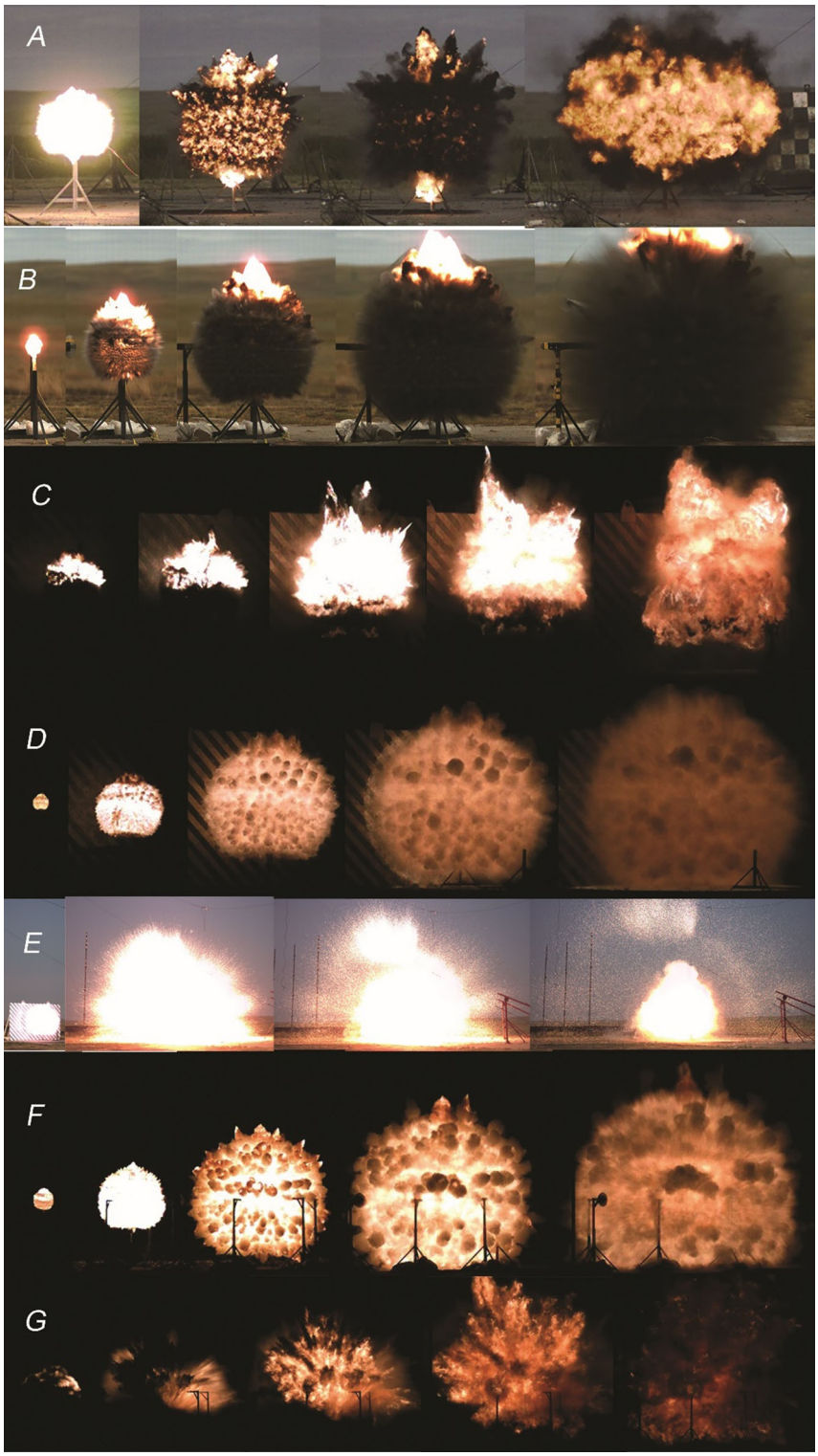

Figure 5. Composite image showing time lapse images of the various particle laden explosives used in the trials: (A) NM ($t = 0.2$, 0.6, 1.0, 31.6 ms), (B) iron particles ($t = 0.1$, 0.4, 0.8, 1.3, 2.5 ms), (C) H-50 aluminum ($t = 0.5$, 1, 5, 10, 20 ms), (D) zirconium ($t = 0.06$, 0.32, 1, 2, 4 ms), (E) zirconium (same trial as in D, but with a wider camera view with daylight exposure and longer times, $t = 2.1$, 33.3, 66.7, 133.3 ms), (F) titanium (TI-109; $t = 0.06$, 0.32, 1, 2, 4 ms), and (G) titanium (TI-104; $t = 1$, 5, 10, 20, 40 ms).

We will now consider the results of the thermocouple temperature measurements for the various charge conditions. Figure 6 shows examples of the temperature histories recorded with 127 μm thermocouples for homogeneous NM charges in comparison with heterogeneous charges containing either inert or reactive particles. The temperature histories are shown at distances of either 1.2 m or 1.5 m from the charge. The highest temperatures were recorded for the charges with Al particles, perhaps due to the highly energetic nature of Al combustion and the relatively long residence time of the Al particles within the fireball, as noted above.

The lowest gas temperatures were recorded for trials with inert iron particles. In this case, the particles act as an effective heat sink and the thermocouple temperature did not rise above 370 K. The observed afterburning of the NM products in Figure 5A for pure nitromethane was not observed when mixed with the iron particles, providing evidence of the heat sink effect of the iron at quenching the post-detonation reaction.

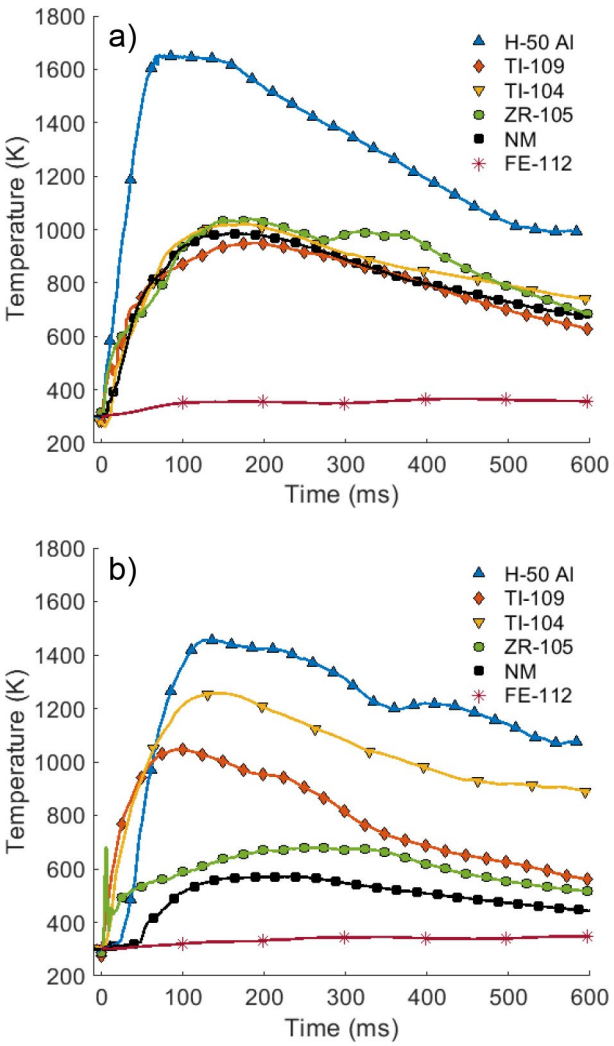

Figure 6. Thermocouple temperatures from various reactive materials at stand-off distances of a) 1.2 m and b) 1.5 m.

4.2 Repeatability of Thermal Profiles

The temperatures recorded at 3 different locations within the fireball are shown for 2 sets of 2 identical trials in Figure 7, which illustrates the degree of variation between trials. One set of trials used charges containing H-50 Al particles and the other set with only sensitized NM.

Close to the charge, the charges with Al generated significantly higher gas temperatures, whereas, at a distance of 1.9 m, which is in the afterburning mixing zone between the combustion products and surrounding air, the temperatures attained by the homogeneous and heterogeneous charges were comparable. The gas temperatures in the fireball for the NM/Al charges remains at elevated levels above 1000 K for durations on the order of 0.5 s. However, the gas temperatures recorded within the fireball are still considerably lower than the temperature of the burning Al particles, estimated earlier with pyrometry to be 2700 ± 200 K at times on the order of 10's of ms [6].

From Figure 7, the thermocouple temperature typically reaches a maximum after several hundred milliseconds. Note that the location of the peak temperature varies from one trial to the next due to the variation in the location of afterburning due to the spatial fluctuations in turbulent mixing.

In general, large spatial non-uniformities in the gas temperature were recorded. This is due to several factors. First, due to the large mass loading of aluminum particles (79 ± 1 % by mass), in many cases the expanding cloud of aluminum particles did not ignite uniformly throughout the cloud, leaving pockets of unburnt particles that burn out over long timescales. Secondly, in addition to the RT instability of the combustion product interface, the particle cloud is also unstable and typically forms coherent clusters of particles. The local gas temperature attained depends on whether a burning jet of particles engulfs a thermocouple gauge (or not).

4.3 Application of the Local Extrema Method (LEM)

Following the discussion in the introduction, whenever the thermocouple temperature exhibits a local maximum, or minimum, the thermocouple temperature is instantaneously identical to the local fluid temperature. By extracting all of the minima and maxima values from the thermocouple temperature traces, instantaneous gas temperatures, at a given location and time, were obtained for the various charge configurations tested and the results are shown tabulated in Table 2.

The variation in the instantaneous temperature measurements obtained using the LEM method given in Table 2

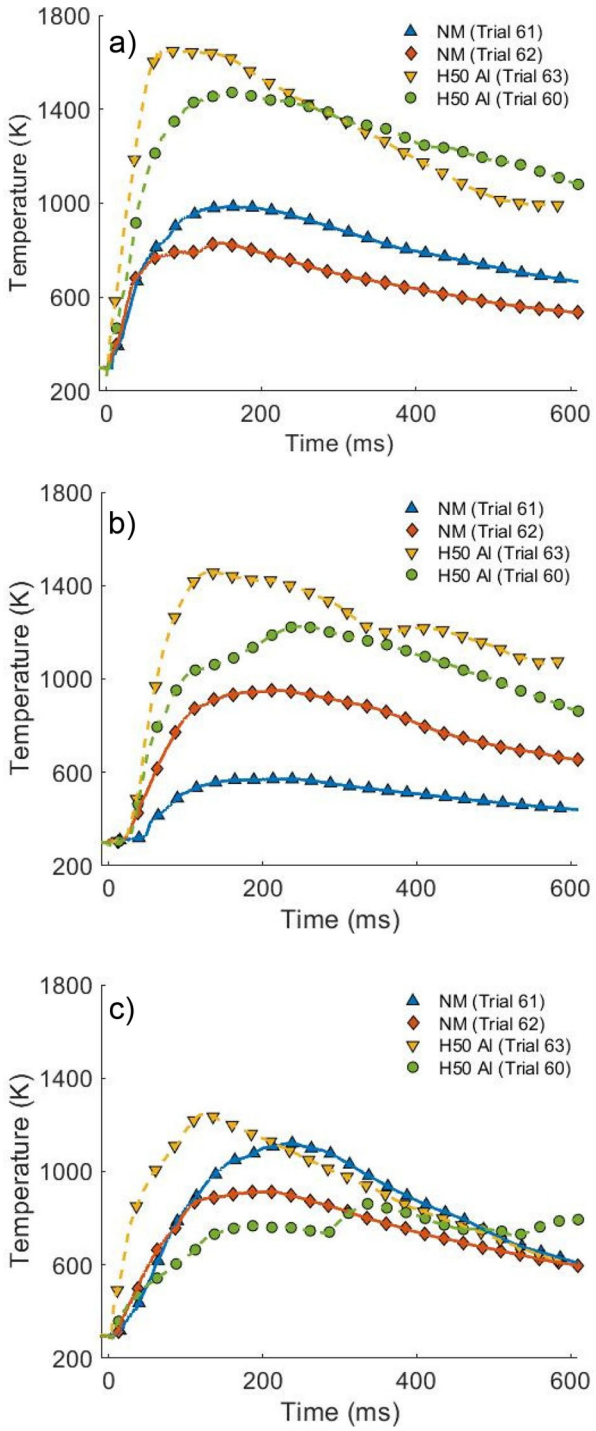

Figure 7. Recorded gas temperatures for two H-50 and two sensitized NM trials at stand-off distances of a) 1.2 m, b) 1.5 m, and c) 1.9 m.

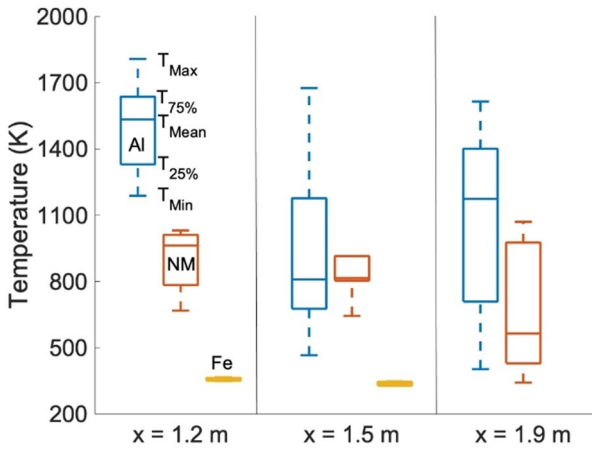

Figure 8. Box plot of local extrema temperatures recorded from trials containing H-50 Al particles at stand-off distances of 1.2 m, 1.5 m, and 1.9 m.

for the baseline trials containing only NM and trials with H-50 Al and FE-112 iron particles are plotted in Figure 8. The box plots shown in this figure provide a statistical representation of the local extrema extracted from the temperature histories at standoff distances of 1.2 m, 1.5 m, and 1.9 m. The plot shows the maximum, minimum, and mean extrema temperature at each location as well as the 75th and 25th quartile based on the range of each local extrema recorded. The results for the iron particles are displayed at standoff distances of 1.2 m and 1.5 m due to the lack of a gauge located at 1.9 m during those trials.

For the baseline charges containing 1 kg of NM alone, from Table 2 and Figure 8 during the period of 100–200 ms after detonation of the charge, gas temperatures within the fireball attain values between 650–1050 K. The maximum temperature observed is considerably lower than the temperature of the condensed products (soot) of 1900 ± 150 K that was measured earlier with optical pyrometry at times on the order of 10–100 ms [6]. The thermocouples are too slow to respond to the very high shocked-air temperatures observed by pyrometry at early times [5, 6]. At the furthest distance from the charge (1.9 m), in some trials very low temperatures were recorded, which indicates that the thermocouple located at a distance of 1.9 m is very close to the maximum extent of the fireball, which is consistent with the video records.

The large variations in extrema temperatures and the locations at which they were recorded for the H-50 Al particle trials are also shown in Figure 8. As noted earlier (see Figures 6, 7), in the near field (1.2 m), the temperatures recorded for the charges with Al particles were significantly higher than the baseline NM charges. However, at a distance of 1.9 m, which is within the mixing zone between the fireball interface and surrounding atmosphere, large gas temperature variations are observed due to spatial variations in the symmetry of the Al particle cloud and degree of complete combustion of the particles. The earlier observation that the inert iron particles act as a heat sink is reflected in the low temperatures recorded and the lack of variation in extrema temperatures from the various trials.

Table 2. Instantaneous temperatures extracted from thermocouple temperature histories using LEM method.

Trial No.	Particles	Distance (m)	Time (ms)	Temperature (K)
05TR32	NM	1.2	106	668
06TR05	NM	1.2	122	1020
06TR62	NM	1.2	144	830
07TR84	NM	1.2	150	768
06TR61	NM	1.2	161	985
05TR33	NM	1.2	189	963
06TR65	NM	1.2	215	1031
06TR65	NM	1.5	91	805
07TR84	NM	1.5	129	644
05TR33	NM	1.5	133	804
05TR32	NM	1.5	194	826
06TR62	NM	1.5	208	915
06TR61	NM	1.5	233	1121
06TR65	NM	1.9	184	1072
05TR32	NM	1.9	217	458
06TR62	NM	1.9	229	945
05TR33	NM	1.9	244	342
06TR61	NM	1.9	247	564
06TR59	H-50 Al	1.2	122	1552
06TR66	H-50 Al	1.2	129	1808
06TR63	H-50 Al	1.2	131	1642
05TR34	H-50 Al	1.2	139	1516
06TR60	H-50 Al	1.2	164	1472
05TR38	H-50 Al	1.2	239	500
05TR35	H-50 Al	1.2	356	1188
06TR66	H-50 Al	1.2	471	1632
05TR35	H-50 Al	1.5	100	1676
05TR39	H-50 Al	1.5	122	1335
06TR66	H-50 Al	1.5	482	1263
06TR63	H-50 Al	1.5	123	1246
06TR66	H-50 Al	1.5	171	1108
05TR38	H-50 Al	1.5	244	1106
05TR41	H-50 Al	1.5	128	979
06TR60	H-50 Al	1.5	335	855
06TR60	H-50 Al	1.5	182	764
05TR41	H-50 Al	1.5	578	751
05TR34	H-50 Al	1.5	372	738
05TR34	H-50 Al	1.5	144	709
06TR58	H-50 Al	1.5	68	644
06TR59	H-50 Al	1.5	598	639
06TR59	H-50 Al	1.5	108	609
05TR41	H-50 Al	1.5	1122	466
05TR41	H-50 Al	1.9	34	1615
05TR39	H-50 Al	1.9	40	1132
06TR58	H-50 Al	1.9	115	403
06TR63	H-50 Al	1.9	130	1456
06TR59	H-50 Al	1.9	182	479
06TR60	H-50 Al	1.9	249	1226
05TR35	H-50 Al	1.9	250	1401
05TR34	H-50 Al	1.9	311	648
05TR38	H-50 Al	1.9	361	1032
05TR35	H-50 Al	1.9	372	1376
06TR63	H-50 Al	1.9	403	1216
06TR66	H-50 Al	1.9	442	1428
05TR39	H-50 Al	1.9	600	862
05TR34	H-50 Al	1.9	683	709
07TR97	Fe-112	0.9	89	326
07TR97	Fe-112	0.9	196	325
07TR97	Fe-112	0.9	301	323
07TR97	Fe-112	1.2	179	355
07TR97	Fe-112	1.2	282	349
07TR97	Fe-112	1.2	435	366
07TR97	Fe-112	1.5	160	328
07TR97	Fe-112	1.5	186	329
07TR97	Fe-112	1.5	342	345
07TR97	Fe-112	1.5	454	338
07TR97	Fe-112	1.5	586	348
07TR86	Ti-109	0.9	188	1447
07TR85	Ti-109	0.9	208	1248
07TR86	Ti-109	1.2	135	1087
07TR85	Ti-109	1.2	192	951
07TR85	Ti-109	1.5	95	1042
07TR86	Ti-109	1.5	106	952
07TR88	Ti-104	0.9	117	1152
07TR89	Ti-104	0.9	159	1523
07TR88	Ti-104	1.2	113	690
07TR89	Ti-104	1.2	183	1019
07TR89	Ti-104	1.2	280	676
07TR89	Ti-104	1.5	144	1265
07TR88	Ti-104	1.5	146	1669
07TR89	Ti-104	1.5	619	918
07TR89	Ti-104	1.5	677	884
07TR101	Zr-105	0.9	92	1017
07TR100	Zr-105	0.9	172	773
07TR101	Zr-105	1.2	167	1261
07TR101	Zr-105	1.2	181	1040
07TR100	Zr-105	1.2	227	1318
07TR101	Zr-105	1.2	312	992
07TR101	Zr-105	1.2	375	978
07TR101	Zr-105	1.2	728	629
07TR101	Zr-105	1.5	64	696
07TR100	Zr-105	1.5	199	845
07TR101	Zr-105	1.5	267	679
07TR101	Zr-105	1.5	695	502

Figure 9 is a similar box plot representation comparing all of the local extrema temperatures from reactive particle (Al, Ti-109, Ti-104, Zr-105) trials at stand-off distances of 1.2 m and 1.5 m. At the distance of 1.2 m, the highest temperatures are recorded for charges with Al particles, whereas the finer Ti particles (Ti-104) generate the lowest temperatures due to the nonuniform dispersal and inefficient particle ignition observed in Figure 5G. At both distances, the particles that are observed from Figure 5 to disperse most uniformly and have the shortest residence time within the combustion products (i.e., Ti-109 and Zr-105) result in the least variation in gas temperatures observed. For these particles, the particles continue to burn as they travel over a large distance and hence deposit the chemical energy released over a much larger volume of gas.

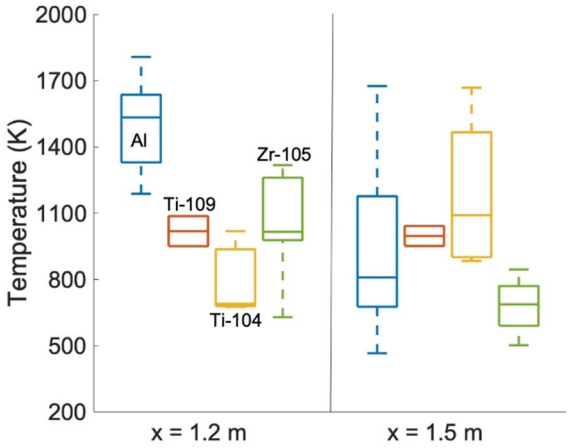

Figure 9. Box plot of local extrema temperatures recorded from trials containing reactive material particles at stand-off distances of 1.2 m, and 1.5 m.

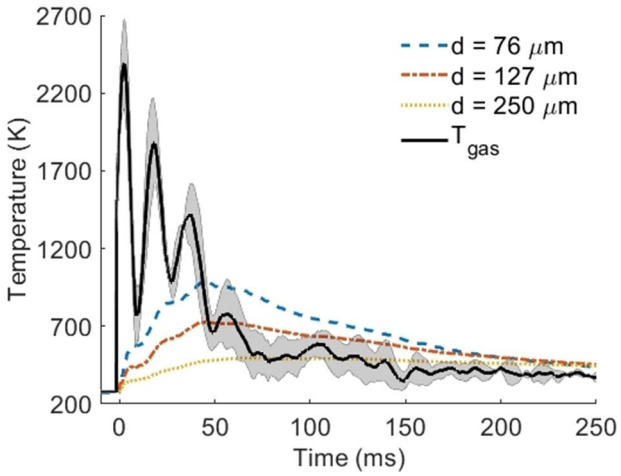

Figure 10. Reconstructed gas temperature from a bare C4 charge with multi-thermocouple sensor head placed 50 cm away. The shaded section represents 80% confidence intervals.

4.4 Application of the Numerical Reconstruction Method (NRM)

The Numerical Reconstruction Method was applied to a similarly posed experiment at the same test location. The multi-thermocouple mount with 3 thermocouples nearby, shown in the bottom left of Figure 4, was used to measure the fireball temperature for a 1 kg bare C4 charge. Type C thermocouples of bead diameters 76 μm (0.003″), 127 μm (0.005″), and 254 μm (0.010″) were placed in the mount approximately 50 cm from the charge. As stated in the analysis section of the numerical reconstruction method, the three recorded temperature traces were used to reconstruct the local gas temperature experienced by the sensor. In particular, the algorithm for reconstructing the gas temperature history from two thermocouple traces described in Section 2.2 above (Eqs. 2–4) is extended to three thermocouples. The third sensor allows for three independent pairs of thermocouple measurements.

When the time constants for the first-order lag equations are found, they are then plugged back into the equations to solve for the true gas temperature T_g. The time-dependent mean of all three traces and the corresponding standard deviation is output from the algorithm. The confidence interval is then calculated using the standard deviation and the corresponding critical values of the two-sided *t*-distribution for a sample size of 3.

Using the procedure described above, the gas temperature was reconstructed for the bare C4 trial noted above and the results are shown in Figure 10, together with the three thermocouple traces. It is visible that the reconstructed temperature exceeds the maximum measured thermocouple temperature by nearly 1200 K. Since the gas temperature experienced by the thermocouples lags behind the real gas temperature, it can be assumed that the real temperature is significantly higher than the measured value due to the sharp rise in the slope of the highest bandwidth, smallest diameter thermocouple. The reconstructed trace is evidence that the calculation of the time derivative, and its use in estimating the time constant, impacts the reconstruction significantly. Another interesting feature is the reconstruction's correlation with the maxima of each thermocouple measurement. This corresponds with the assumption inherent in the LEM method that at minima and maxima of a thermocouple trace, the measurement is unequivocally equal to the local gas temperature. The domination of the time derivative term in the numerical reconstruction leads to the large oscillations apparent in the reconstructed temperature.

The timing of the temperature oscillations in Figure 10 is consistent with the interaction of the primary blast (initial peak) and the arrival of the reflected shock from a nearby wall with the fireball (second and third peak). The shocks enhance the mixing and afterburning of detonation products at the combustion product contact surface and thus increase the local temperature. Measurements of pressure spikes at a gauge located at a similar radial distance from the charge correspond with the temperature peaks, but the reconstruction method likely exaggerates the amplitude of these temperature oscillations due to the assumption that the thermocouple time constants do not vary in time. In reality, the thermocouple time constants will vary due to changes in the rate of heat transfer as a result of the change in flow speed induced by the shocks. This is not accounted for in the reconstruction method in this paper and is the subject of future work.

5 Conclusions

The main conclusions of the present experiments are as follows.

The utility of thermocouples for gaining information regarding the temperature field within fireballs from multiphase explosives has been demonstrated. Although the thermocouple temperature lags behind the ambient gas temperature, when the thermocouple temperature exhibits a local maximum or minimum, the thermocouple temperature is coincident with the local gas temperature and provides an unambiguous measure of fireball gas temperature, although at a limited number of spatial and temporal points. Additionally, the implementation of the Numerical Reconstruction Method provides insight into the local gas temperature experienced by the thermocouple throughout a test.

Gas temperatures within metalized fireballs are, in general, lower than the temperature of the burning particles themselves. Large spatial variations in the temperature field are due to several factors, including incomplete reaction of the particles and the formation of localized particle jets during explosive dispersal. For charges containing sensitized NM, gas temperatures up to about 1100 K were observed after several 100's of milliseconds. With added aluminum particles, gas temperatures up to about 1800 K were observed in some cases up to 0.5 s after detonation of the charge. The highest gas temperatures in the fireballs were observed for aluminum and fine titanium particles, which disperse in a non-uniform manner, ignite in local regions, with flame propagation through the particle cloud over milliseconds or even 10's of milliseconds. These particles continue to burn for some time within the fireball or nearby. Conversely, large titanium particles and zirconium particles ignite promptly within the fireball and burn heterogeneously, disperse uniformly along ballistic trajectories, and have a shorter residence time within the fireball. As a result, for these particles, the gas temperature attained within the fireball is smaller with also a smaller temperature variation.

Future work should pursue the development of local laser absorption measurements to obtain a continuous measure of fireball gas temperature. The possibility of localized particle density measurements using laser scattering has been demonstrated [22], and a similar gauge design may be considered, although such a gauge would by necessity measure an average temperature over the distance between the laser emitter and collector.

Acknowledgments

The authors acknowledge the assistance of Francois Jetté in performing the thermocouple temperature test shown in Figure 1. The authors would like to thank D. Boechler for assistance with the data acquisition system, S. Trebble for high-speed photography support, and the Field Operation Section for their assistance in the performance of the experimental trials at DRDC Suffield. Support for this work was provided by DRDC Suffield, and the Defense Threat Reduction Agency under contract HDTRA1-18-1-0011 (program manager Jeffery Davis).

Data Availability Statement

Data available on request from the authors.

References

[1] Q. Pontalier, J. Loiseau, S. Goroshin, D. L. Frost, F. Zhang, Effect of particle loading on the blast wave from a metalized explosive, *25th International Symposium on Military Aspects of Blast and Shock (MABS 25)*, The Hague, Netherlands, September 24–28, **2018**, 1–20.

[2] D. L. Frost, F. Zhang, S. Murray, S. McCahan, Critical conditions for ignition of metal particles in a condensed explosive, *Proc. of 12th International Detonation Symposium*, San Diego, CA, USA, Aug. 11–16, **2002**.

[3] Q. Pontalier, J. Loiseau, S. Goroshin, F. Zhang, D. L. Frost, Blast enhancement from metalized explosives, *Shock Waves*, in press, **2020**.

[4] D. L. Frost, S. Goroshin, R. C. Ripley, F. Zhang, Temperature measurements in a fireball from a metalized explosive, *24th International Symposium on Military Aspects of Blast and Shock (MABS 24)*, Halifax, NS, Canada, September 18–23, **2016**.

[5] T. Ogura, K. Okada, T. Abe, K. Wakabayashi, K. Ishikawa, E. Kuroda, T. Matsumura, Y. Nakayama, M. Yoshida, Pyrometry study of fireballs generated upon the explosion of TNT. *Proc. 34th Ann. Conf. ICT.*, Karlsruhe, Germany, June 24–27, **2003**, 18.

[6] S. Goroshin, D. L. Frost, J. Levine, A. Yoshinaka, F. Zhang, Optical pyrometry of fireballs of metalized explosives. *Propellants Explos. Pyrotech.* **2006**, *31*, 169. doi: 10.1002/prep.200600024.

[7] J. R. Carney, J. S. Miller, J. C. Gump, G. I. Pangilinan. Time-resolved optical measurements of the post-detonation combustion of aluminized explosives . *Rev. Sci. Instrum.* **2006**, *77*, 063103. doi: 10.1063/1.2200766.

[8] N. Glumac, H. Krier, P. Lynch, J. Mott Peuker, Optical spectroscopy of fireballs from metallized reactive materials, *48th AIAA Aerospace Sciences Meeting Including the New Horizons Forum and Aerospace Expostition*, Orlando, FL, USA, January 4–7, **2010**, *695*. doi: 10.2514/6.2010–695.

[9] P. Lynch, H. Krier, N. Glumac, A correlation for burn time of aluminum particles in the transition regime, *Proc. of the Combustion Institute* **2009**, *32*, 1887. doi: 10.1016/j.proci.2008.06.205.

[10] S. Goroshin, J. Mamen, A. J. Higgins, T. Bazyn, N. Glumac, H. Krier, Emission spectroscopy of flame fronts in aluminum suspensions. *Proc. of the Combustion Institute* **2007**, *31*, 2011. doi: 10.1016/j.proci.2006.07.175.

[11] M. Soo, N. Glumac, Ultraviolet absorption spectroscopy in optically dense fireballs using broadband second-harmonic generation of a pulsed modeless dye laser. *Appl. Spectrosc.* **2014**, *68*, 5. doi: 10.1366/13–07276.

[12] C. Murzyn, A. Sims, H. Krier, N. Glumac, High speed temperature, pressure, and water vapor concentration measurement in explosive fireballs using tunable dioide laser absorption spectroscopy, *Optics and Lasers in Engineering* **2018**, *110*, 186. doi: 10.1016/j.optlaseng.2018.06.005.

[13] M. Soo, A. Sims, J. Cerow, J. Lightstone, C. Murzyn, N. Glumac, J. Ott, M. DeMagistris, N. Sinha, Measurement of temperature

and water vapor concentration using laser absorption spectroscopy in kilogram-scale explosive fireballs, *Proc. of the 21st APS Topical Conference on Shock Compression of Condensed Matter*, Portland, OR, USA, June 16–21, **2019**, *64*.

[14] B. W. Asay, S. F. Son, P. M. Dickson, L. B. Smilowitz, B. F. Henson, An investigation of the dynamic response of thermocouples in inert and reacting condensed phase energetic materials. *Propellants Explos. Pyrotech.* **2005**, *30*, 199. doi: 10.1002/prep.200500006.

[15] F.-X. Jetté, S. Goroshin, D. L. Frost, F. Zhang, Shock initiation of powder mixtures of aluminum with dense metal oxides, *Shock Compression of Condensed Matter*, AIP Conf. Proc. 1426, Chicago, IL, USA, June 26–July 1, **2011**, *279*. doi: 10.1063/1.3686273.

[16] M. Tagawa, T. Shimoji, T. Ohta, A two-thermocouple probe technique for estimating thermocouple time constants in flows with combustion: *In Situ* parameter identification of a first-order lag system, *Rev. Sci. Instrum.* **1998**, 69, 3370. doi: 10.1063/1.1149103.

[17] P. Julien, J. Vickery, S. Goroshin, D. L. Frost, J. M. Bergthorson, Freely-propagating flames in aluminum dust clouds. *Combust. Flame* **2015**, *162*, 4241. doi: 10.1016/j.combustflame.-2015.07.046.

[18] P. A. Gorry, General least-squares smoothing and differentiation by the convolution (Savitsky-Golay) method, *Anal. Chem.* **1990**, *62*, 570. doi: 10.1021/ac00205a007.

[19] M. Tagawa, T. Ohta, Two-thermocouple probe for fluctuating temperature measurement in combustion – rational estimation of mean and fluctuating time constants, *Combust. Flame* **1997**, *109*, 549. doi: 10.1016/S0010-2180(97)00044–8.

[20] F. Zhang, D. L. Frost, P. A. Thibault, S. B. Murray, Explosive Dispersal of Solid Particles. *Shock Waves* **2001**, *10*, 431.

[21] D. L. Frost, Z. Zarei, F. Zhang, Instability of Combustion Products Interface from Detonation of Heterogeneous Explosives, *20th International Colloquium on the Dynamics of Explosions and Reactive Systems*, Montreal, QC, Canada, July 31–August 5, **2005**.

[22] S. Goroshin, D. L. Frost, R. Ripley, F. Zhang, Measurement of particle density during explosive particle dispersal, *Propellants Explos. Pyrotech.* **2016**, *41*, 245. doi: 10.1002/prep.201500262.

Manuscript received: December 17, 2020
Revised manuscript received: January 28, 2021
Version of record online: March 9, 2021

